Supplementary Information

Resonant transport in a highly conducting single molecular junction via metal-metal bond

Biswajit Pabi[1], Štepán Marek[2], Adwitiya Pal[3], Puja Kumari[4], Soumy Jyoti Ray[4], Arunabha Thakur[3], Richard Korytár[2], and Atindra Nath Pal[1*]

[1]Department of Condensed Matter Physics and Material Sciences, S. N. Bose National Centre for Basic Sciences, Sector III, Block JD, Salt Lake, Kolkata 700106, India.
[2]Department of Condensed Matter Physics, Faculty of Mathematics and Physics, Charles University, 121 16, Prague 2, Czech Republic
[3]Department of Chemistry, Jadavpur University, Kolkata-700032, India.
[4]Department of Physics, Indian Institute of Technology Patna, Bihar- 801106, India.

Contents:-

1. Characterization of molecules:

(a) 1,1′-bis(aminomethyl)ferrocene

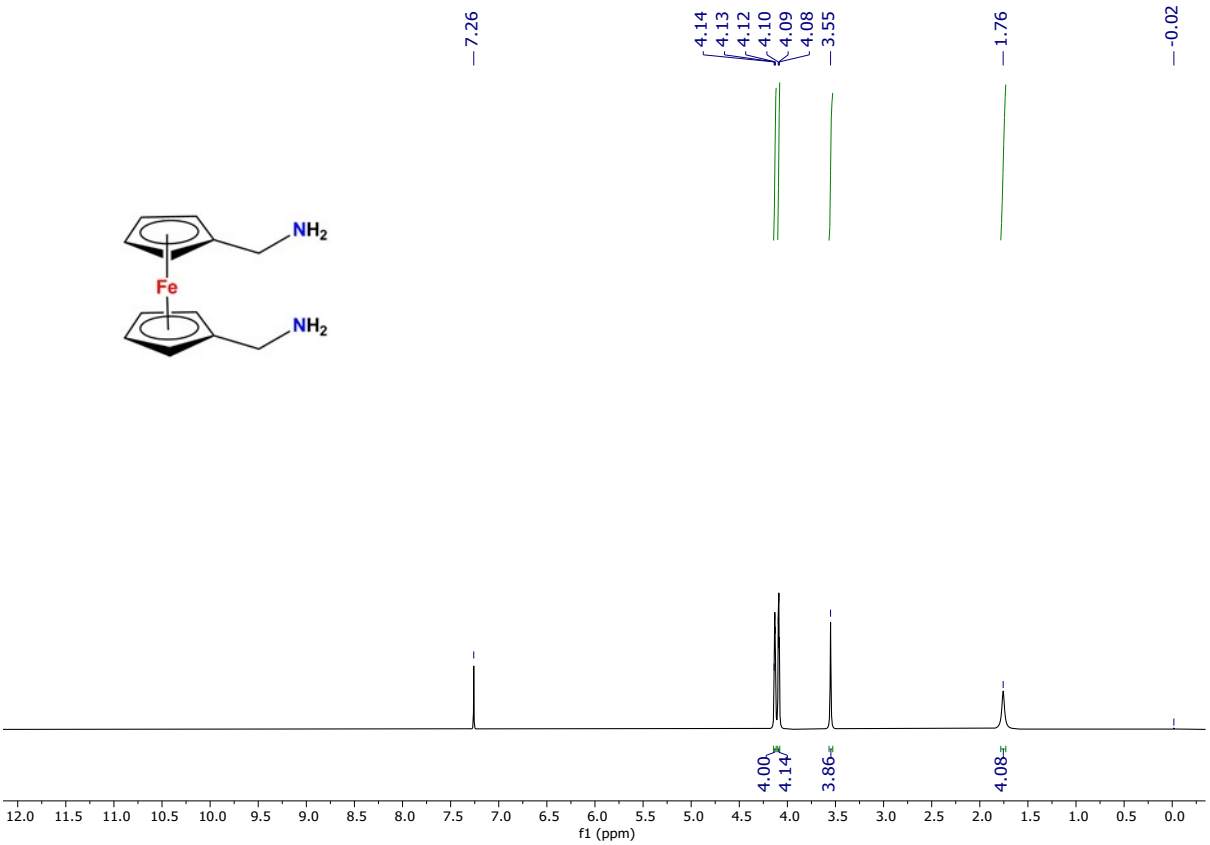

Figure S1: *^{1}H NMR spectrum of 1,1'-bis(aminomethyl)ferrocene in $CDCl_3$.*

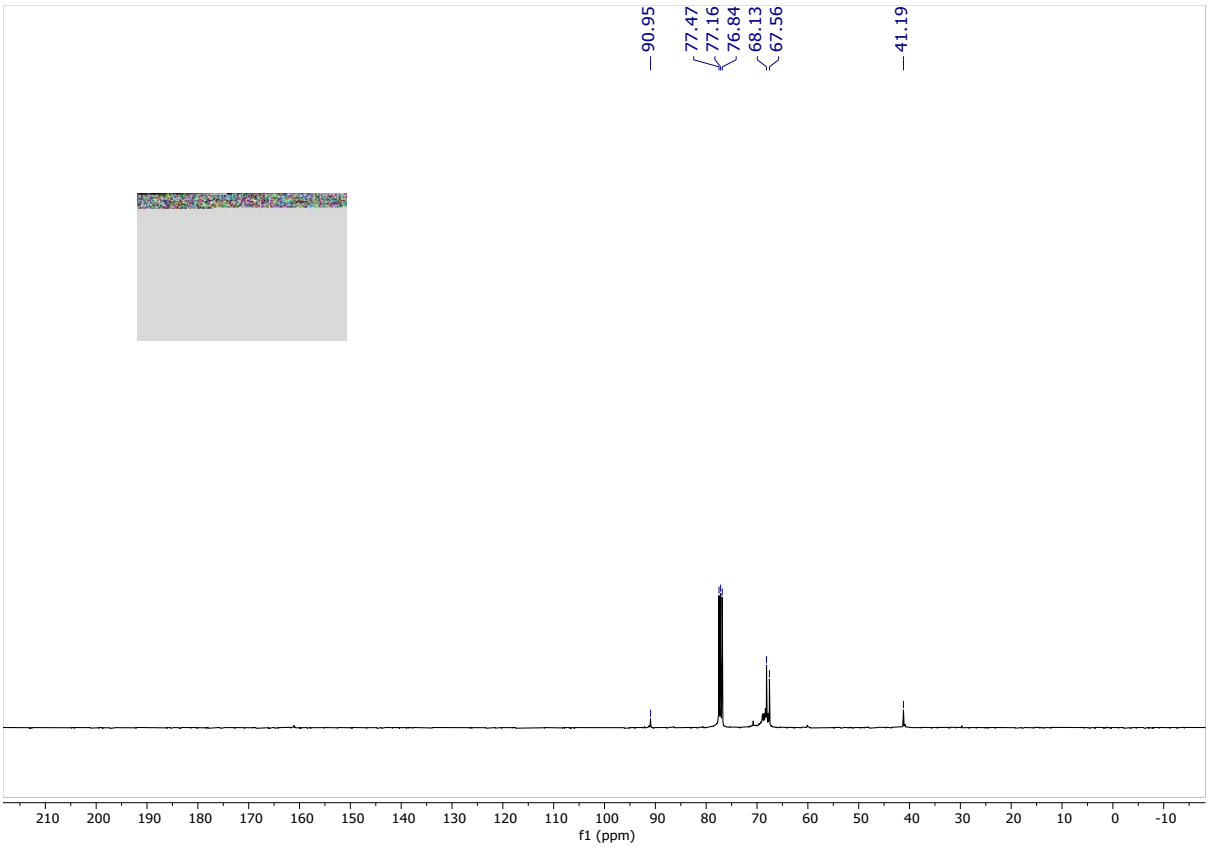

Figure S2: *^{13}C NMR spectrum of 1,1'-bis(aminomethyl)ferrocene in $CDCl_3$.*

(b) 1,1'-dicyanoferrocene

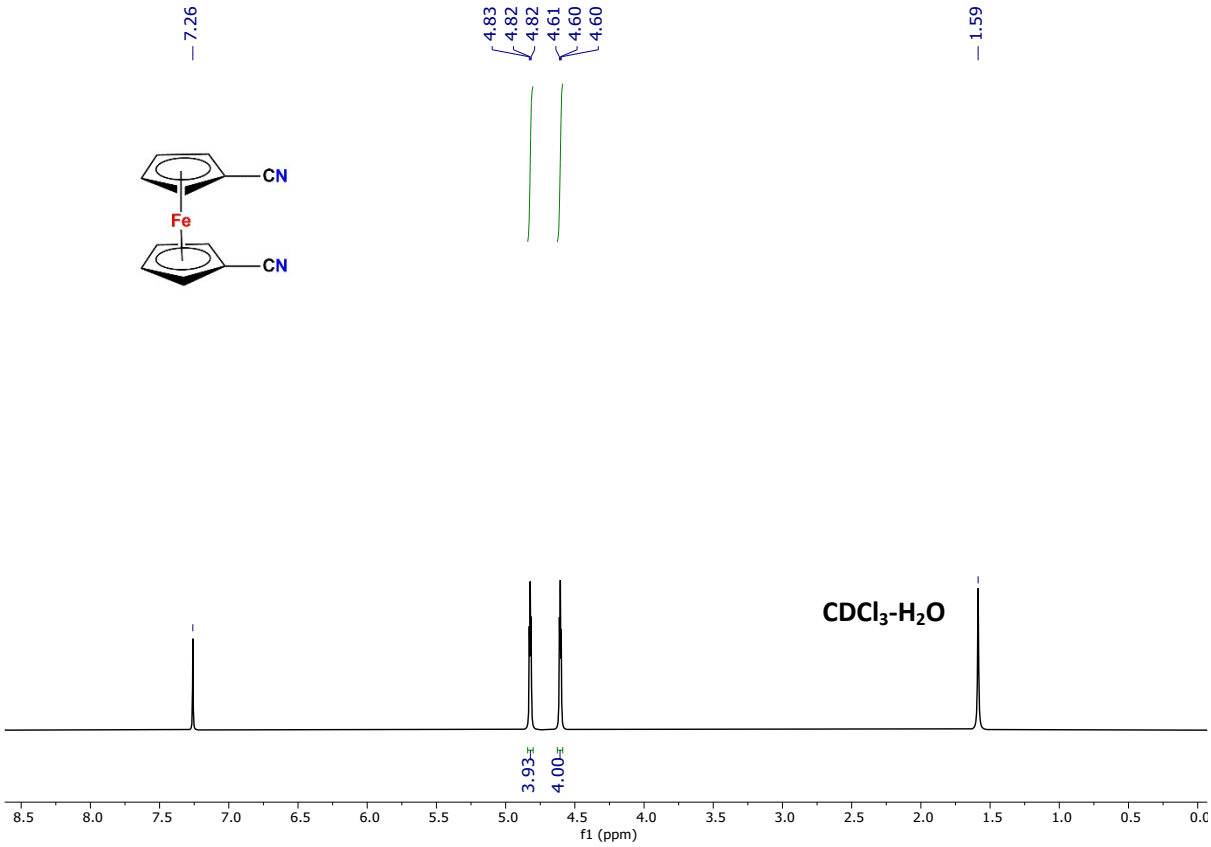

Figure S3: *^{1}H NMR spectrum of 1,1'-dicyanoferrocene in $CDCl_3$.*

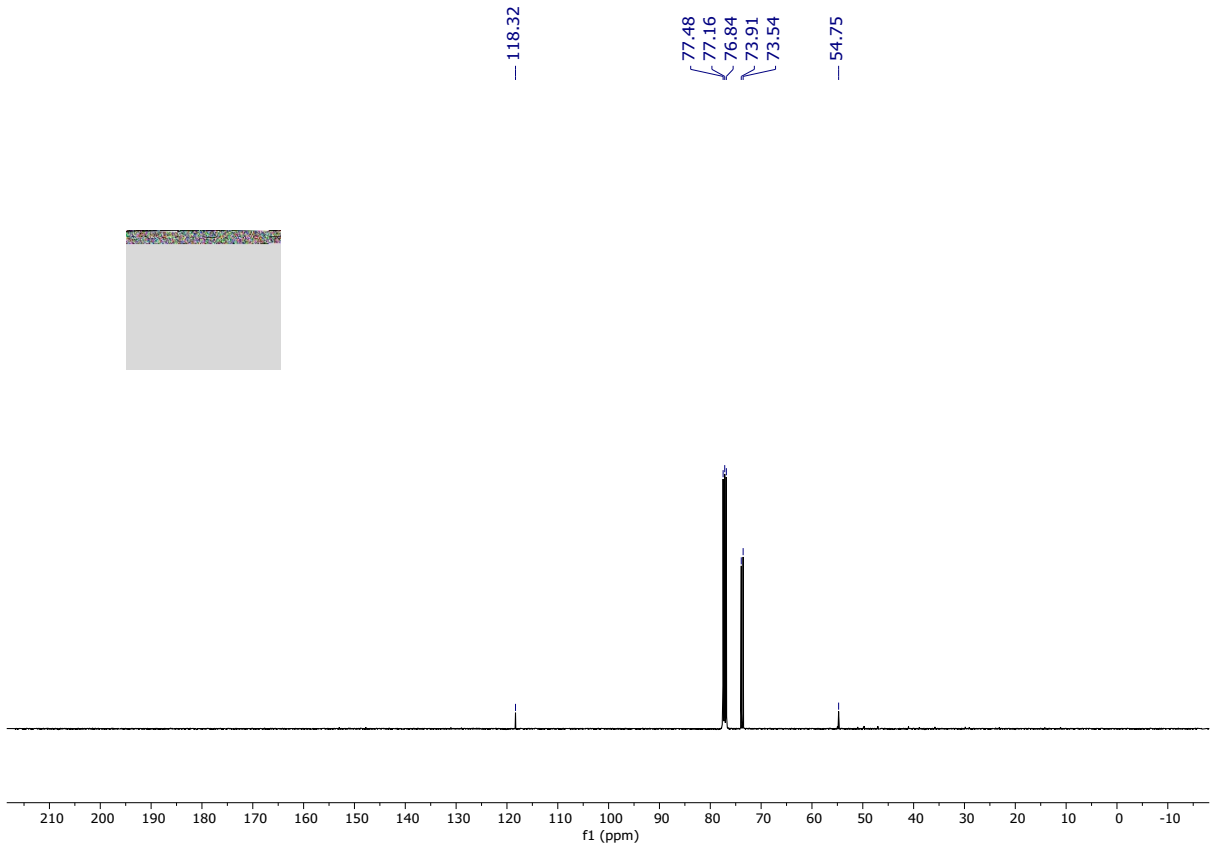

Figure S4: *^{13}C NMR spectrum of 1,1'-dicyanoferrocene in $CDCl_3$.*

2. Analysis tools of experimental data:

(a) 1D conductance histogram

In case of break junction experiment, conductance of the junction is measured as a function of electrode separation, starting from few tenths of atom to the breaking of the junction, by a small and constant increment of electrode separation. A complete measurement cycle is called a *conductance traces* and thousands or even more such traces are collected to look into the junction statistically. Before entering into the next cycle, electrodes are always crashed up to few atoms to delete the memory from previous cycle. In each cycle, junction evolves via series of elastic and plastic deformation leading to a unique configuration, which is beyond to probe experimentally. Thus, statistical analysis of large traces is critically important to identify the most possible scenario. This has been performed by creating conductance histogram[1] which presents distribution of conductance values collected from bulk number of traces. Consequently, when junction exhibits constant conductance values with respect to stretching (i.e. conductance plateaus), many values will add up to a small range of conductance and reflected as a peak in the histogram. Peaks in the histogram are fitted to calculate the most probable conductance values.

(b) 2D conductance-distance histogram and average traces

As mentioned earlier, conductance of the junction is recorded as a function of electrode separation. However, conductance histogram provides only the conductance value, ignoring information

related to the conductance in conjugation with electrode separation or distance. 2D conductance-distance histogram[2,3] is thus created to check the correlation of conductance and distance in a statistical manner. 2D conductance- distance histogram is constructed by following the way: first a conductance value is assigned for each traces as the origin of the distance axis i.e. zero distance point (for our case it is at 2 G_0). Each point in the traces is then contributes to one of the 2D bins of the histogram, defined by conductance and distance from the starting point. The resulting histogram can then be considered as a stack of many traces, placed on top of each other and is helpful to determine the most common feature during stretching.
Average traces for a conductance peak is prepared by calculating most probable conductance values in a certain conductance range, defined by the two local minima around the peak. This gives an additional information regarding the evolution of the junction. Linear fitting of the average traces yields the slope, useful to get an intuitive understanding about the metal-molecule coupling.

(c) Stretching-Length histogram

Stretching length is defined as the difference between two absolute distance values, corresponding to a conductance G_i (= 0.5 G_0; our case) to a desired conductance value G_f. In our case, G_f is assigned at the one order of magnitude beneath the most probable conductance value of the corresponding conductance peak. Stretching length histogram is thus presents the distribution of stretching length, obtained from each traces. Most probable stretching length is calculated by Gaussian fitting of the histogram, which is an indicative of the stability of the junction[4]. Moreover, detailed analysis of stretching length histogram paves the way to quantify the junction formation probability[5].

(d) Correlation analysis

Correlation analysis, introduced by the Makk and coworkers[6], is an extremely useful tool to detect the several features of junction formation and evolution, which cannot be accessible using conventional conductance histogram. To obtain the statistical relation between different junction configurations having its characteristics conductance value, correlation parameter can be defined as,

$$C_{m,n} = \frac{< \delta N_m(r) * \delta N_n(r) >_r}{\sqrt{< [\delta N_m(r)]^2 >_r * < [\delta N_n(r)]^2 >_r}}$$

Where $N_m(r)$ and $N_n(r)$ are the number of data points in the m^{th} and n^{th} bin of the given trace r. $\delta N_{m/n}(r) = N_{m/n}(r) - < N_{m/n}(r) >$ is the deviation from the mean value. Let's discuss the value of $C_{m,n}$ along with its physical significance-
(i) $C_{m,n}$ 0; Configurations are statistically independent.
(ii) $C_{m,n} \neq 0$; Configurations are statistically dependent and type of dependency is determined by the sign of the function. Positive values of $C_{m,n}$ leads to the positive correlation and for these cases configurations either appear or disappear together. Negative value of the function indicate negative correlation and more than average counts in one configuration is supported by the less than average counts in another configuration. It may also happen that formation of one configuration resists the formation of other.

Further details about the correlation analysis is described in reference 6. Using this method, a correlation map is drawn for arbitrary conductance pairs G_m and G_n. Two axis corresponds to the two conductance values and color illustrates $C_{m,n}$.

3. Additional experimental data:

(a) Control experimental data

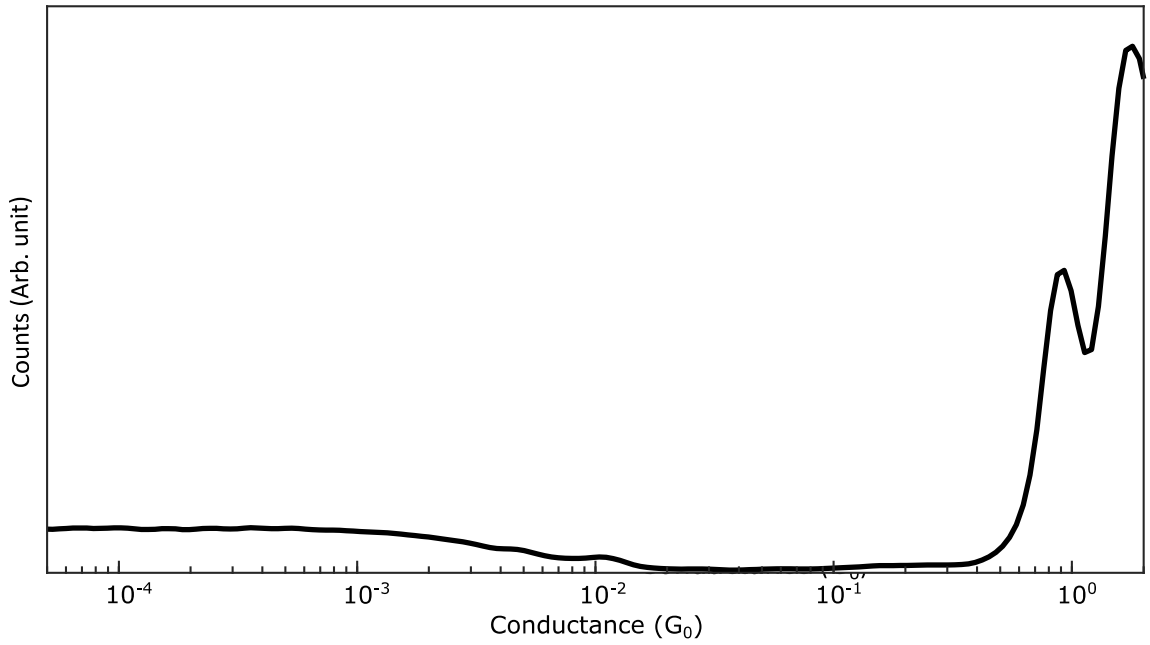

Figure S5: *Conductance histogram constructed from 3000 consecutive conductance traces, recoded for the junction exposed to dichloromethane (DCM) solvent during breaking. Characteristics molecular signature is absent here, similar to reference 7.*

(b) Bias dependent conductance histogram of Au/ferrocene

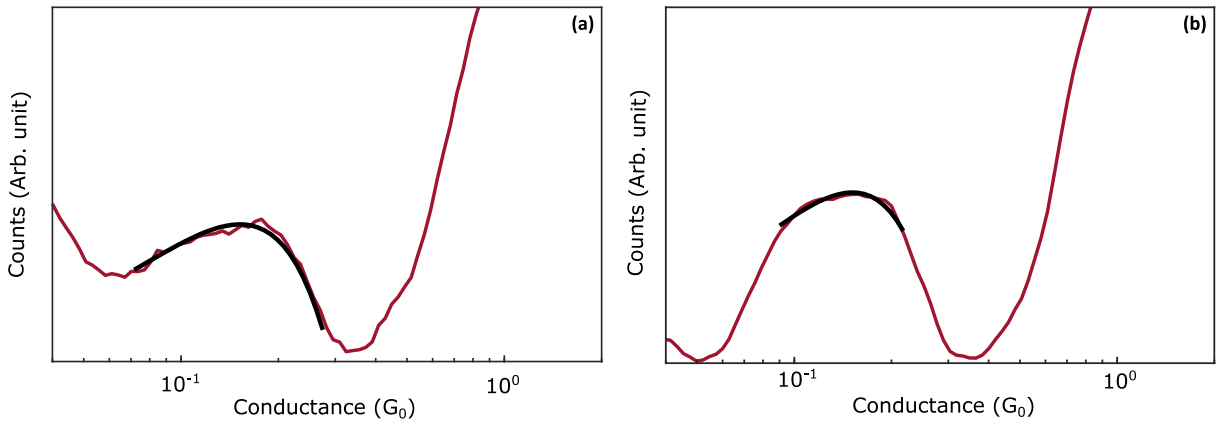

Figure S6: *Conductance histogram of Au/ferrocene/Au junction in logarithmic scale for two different bias voltage 20mV (a) and 50mV (b) where black dash dot line represents the Gaussian*

fitting of the corresponding molecular peak with peak value (1.40 ± 0.02) × 10^{-1} G_0 and (1.60 ± 0.01) × 10^{-1} G_0.

(c) Precursor configuration

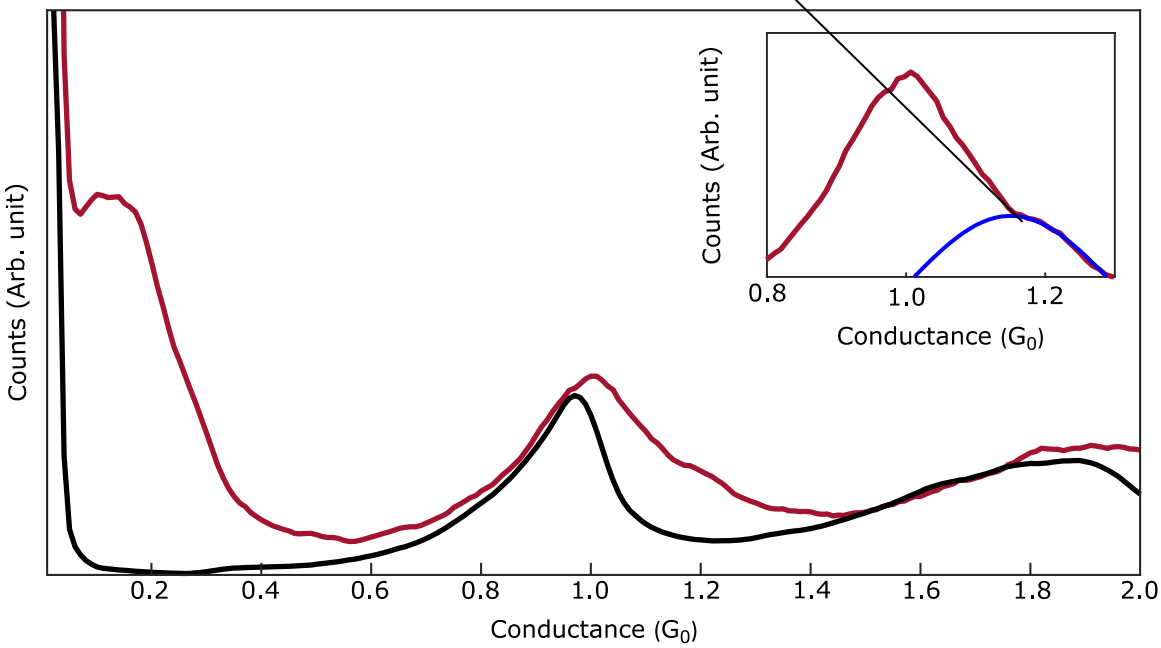

Figure S7: *Conductance histogram constructed from the conductance traces with (red) and without (black) molecular features. Inset: Zoomed view of the same histogram where blue dash-dot line presents the Gaussian fitting of the corresponding precursor peak which yields a maxima at 1.18 ± 0.02 G_0.*

(d) Conditional analysis

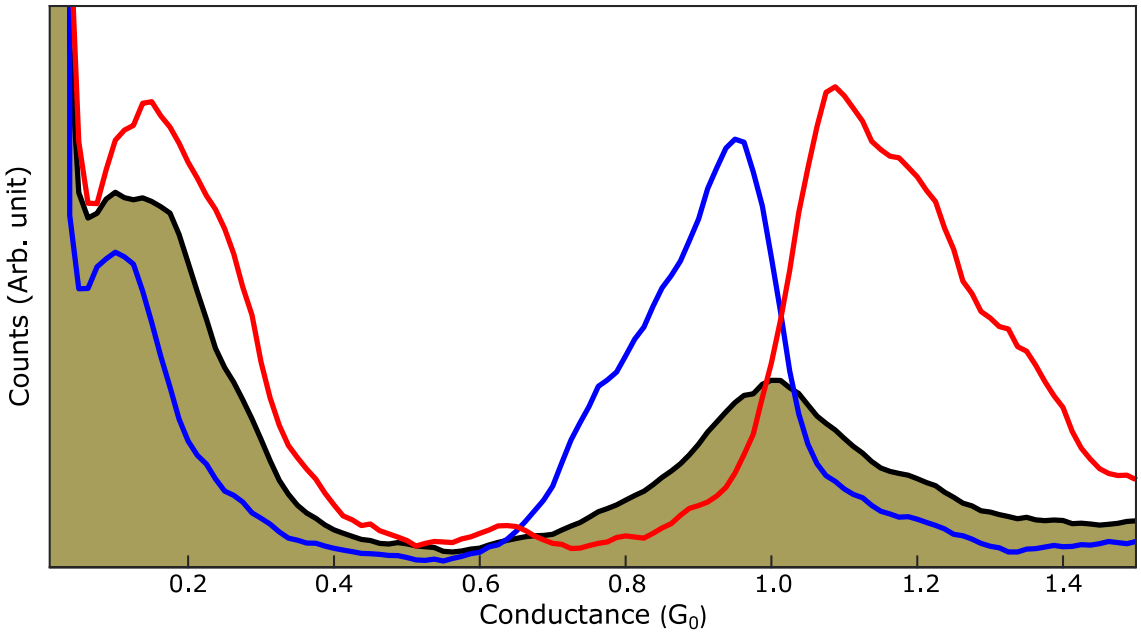

Figure S8: Conditional histograms for selected traces with larger than average length in different regions: R1- molecular conductance region (Red) and R2 - single atomic contacts region (Blue). As a reference the yellowish area graph shows the histogram for all traces.

4. Additional theoretical results

(a) Binding energy curve

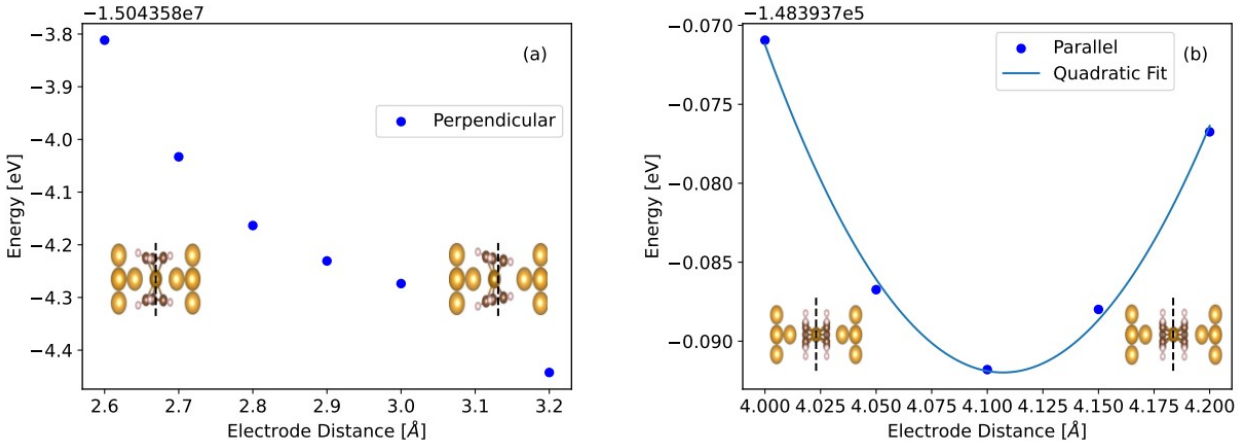

Figure S9: *(a-b) Energy of the extended molecule for different distances of the electrodes from the molecule. For perpendicular geometry (a), no clear minimum is observed for distances around 2.8 Å. However, the molecule occupies a symmetric junction position only for electrodes at this distance or closer. Asymmetric tilting of molecule towards one electrode is illustrated in detail of the junction geometry. For parallel geometry (b), the minimum is observed and the energy dependence is relatively weak. For these positions of electrodes, molecule always forms a symmetric junction.*

(b) Molecular orbitals of free ferrocene

Ferrocene without presence of electrodes has HOMO and LUMO, with HOMO being the dominant transport state.

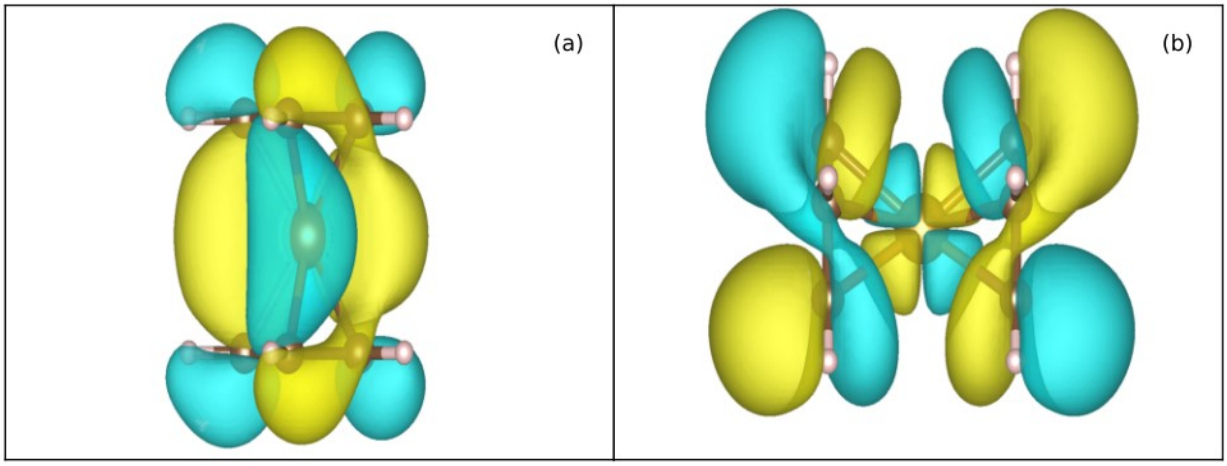

***Figure S10**: (a-b) The highest occupied molecular orbital (HOMO) for free ferrocene (a) and lowest unoccupied molecular orbital (LUMO) for the same molecule (b). The LUMO state is present on the ferrocene extended molecule, as shown in figure 5a-b.*

(c) Conductance of perpendicular and parallel geometry with applied voltage

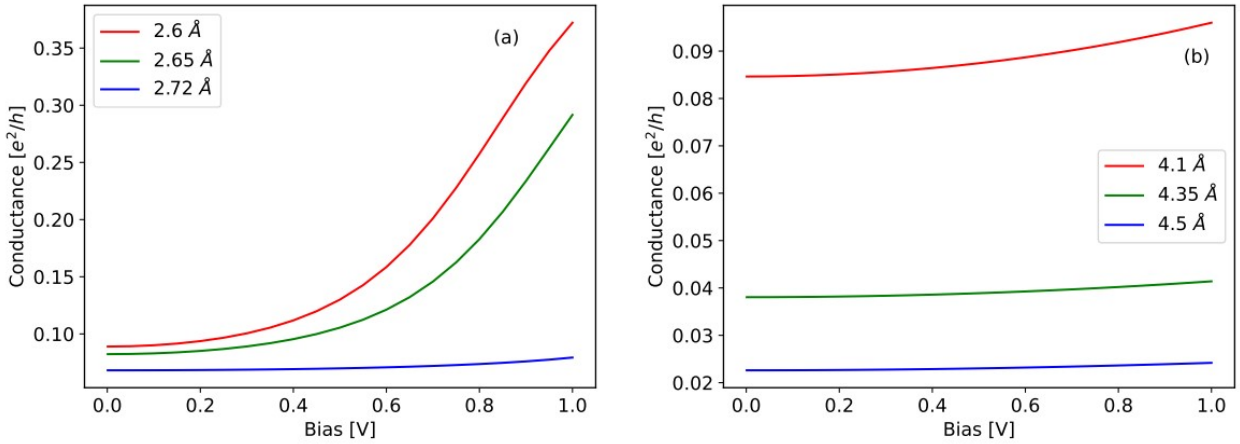

***Figure S11:** (a-b) Conductance (nominal, i.e., current divided by voltage) calculated as integral of the transmission function with transport window kernel. For perpendicular geometry (a), the broadening of the transport window by increased bias voltage leads to significant conductance – the window now encompasses a transmission function peak. For parallel geometry (b), voltage applied would need to be larger to achieve the same conductance as in perpendicular geometry.*

(d) Effect of ring rotation of Cp rings on transmission

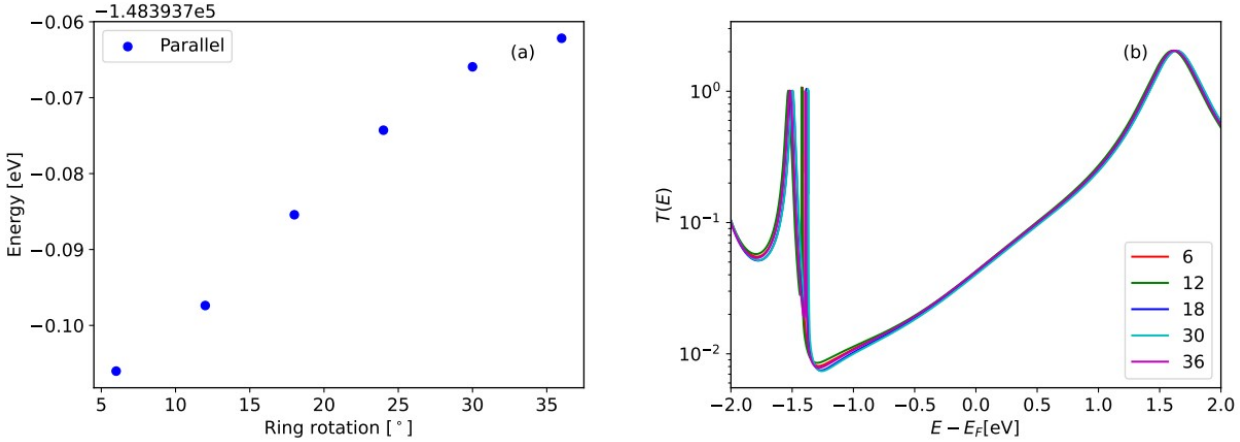

***Figure S12**: (a) Energy of the extended molecule in parallel geometry for different relative rotations of the cyclopentacene rings (0° would represent eclipsed rings). Energy scale is about 40 meV, which is accessible at room temperature. However, the ring rotations have no discernible influence on the shape of transmission function. Hence, only a single relative position of the rings is considered in rest of the text.*

(e) Transmission function of perpendicular and parallel geometry

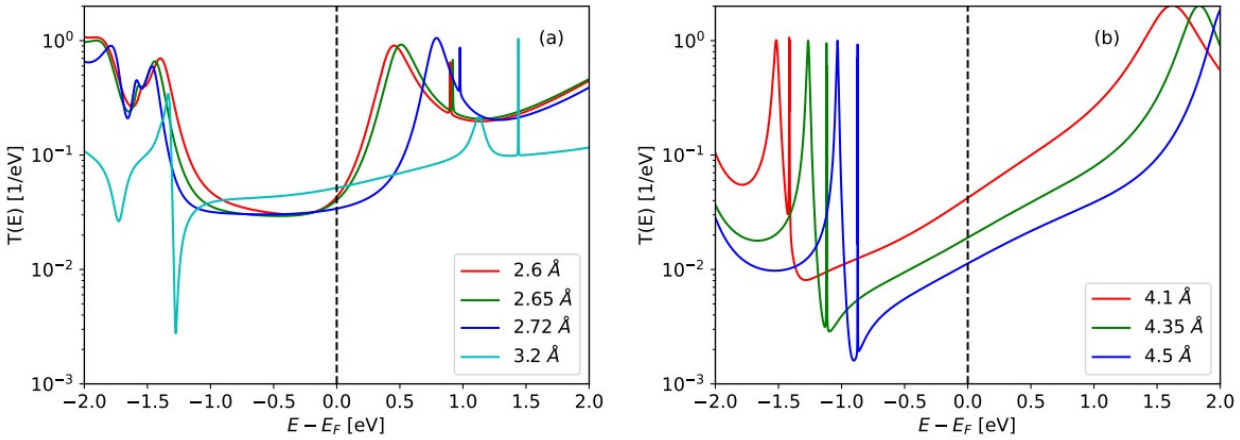

Figure S13*: (a-b) Transmission functions with varying distance of electrodes from the junction centre in perpendicular (a) and parallel (b) geometries of ferrocene molecular junction. For smaller distance, the transmission increases overall, as the overlap of the orbitals increases. Furthermore, peaks tend to shift towards lower energy as the distance decreases. Calculations for parallel geometry are done in TURBOMOLE, for perpendicular geometry, the calculations are done in FHI-AIMS with exception of calculation at 3.2 Å, which is also done in TURBOMOLE – hence wee see that main features of the transmission function are same in TURBOMOLE and in FHI-AIMS.*

(f) Influence of Van der Waals correction and nature of adsorption

We investigate the bond energy in the following way – we calculate the DFT total energy of molecule + electrodes system (extended molecule), $E_{||}$ for parallel geometry (at 4.1 Å) and $E_{\perp}$ for perpendicular geometry (at 2.8 Å) with Van der Waals/dispersion corrections. Then the energy of the same system without the central molecule (electrodes only) $E_{||/\perp,E}$ and the energy of the ferrocene molecule alone (in gas phase), E_g are subtracted, resulting in the estimate of bond energy. Same analysis is carried out for the system without Van der Waals/dispersion corrections, using energy of the extended molecule without dispersion $E_{||/\perp,N}$, energy of electrodes without dispersion $E_{||/\perp,E,N}$ and energy of gas phase ferrocene without dispersion $E_{g,N}$. Results are summarized in Table S1.

We can see that at the given distance, the perpendicular geometry is stabilised by Van der Waals interaction – without it, the bond is not energetically favourable to dissociated state.

Name of the calculation	**Energy, perpendicular (x = ⊥) [eV]**	**Energy, parallel (x=||) [eV]**
Bond energy with VdW (E_x-$E_{x,E}$ - E_g)	-0.66	-1.61

Bond energy without VdW ($E_{x,N} - E_{x,E,N}$-$E_{g,N}$)	0.11	-0.52

Table S1: *Bond energy for the perpendicular and parallel geometries. The used electrode distance is 2.8 Å for perpendicular and 4.1 Å for parallel calculations. For perpendicular geometry, FHI-AIMS program was used, for parallel geometry, TURBOMOLE program was used.*

(g) Local Density of States on the Iron Ion

The local density of states (LDOS) is calculated as a projection of spectral density operator onto the basis of atomic orbitals of a given atom/ion[9]. For a Green's function *G(E)* in the basis of atomic orbitals, local density of states *ρ(E)* for set of chosen orbitals *I* is given as

$$\rho(E) = \frac{-1}{\pi} \sum_{i \in I} IG_{ii}(E)$$

In our case, since we claim that the transport occurs through the metal-metal bond in the perpendicular geometry, it is reasonable to investigate the LDOS on the iron ion at the centre of the ferrocene molecule. The calculation is carried out in the AITRANSS program. The resultant LDOS in both parallel and perpendicular geometry is shown in Fig. S14. Compare these results with the transmission curves presented in Fig. 5 in the main text – the features present in the transmission function are also present in the LDOS.

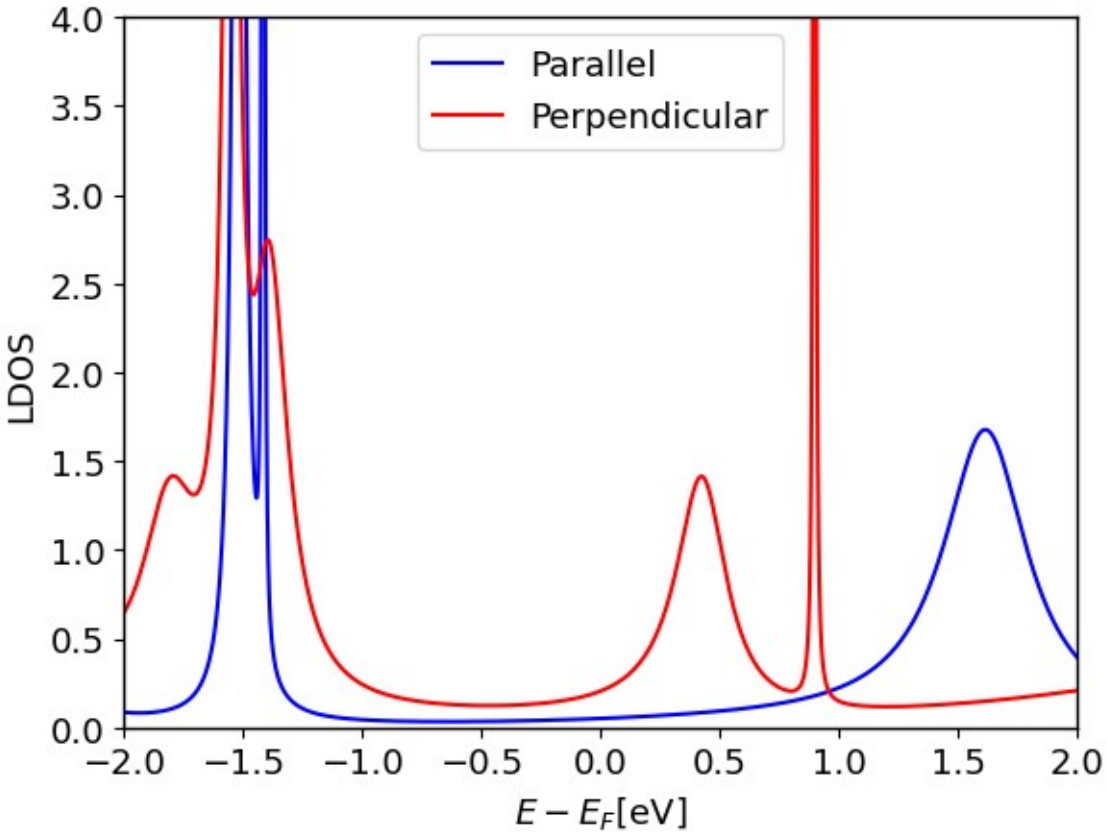

Figure S14: *The local density of states (LDOS) on the iron ion at the centre of the ferrocene molecule. In the parallel geometry, the LUMO transport state is further away from the Fermi energy than in the perpendicular geometry. The apex-to-iron distance were 2.6 Å in perpendicular geometry and 4.1 Å in parallel geometry. The contributions to transport are different from different states, but their location is similar to location of resonances in the transmission curve.*

(h) Stability of Observables – Basis Set Size and Ad-Atoms

Two considerations should be taken into account when determining the convergence behaviour of the observables derived from the ab-initio calculations. Firstly, we should be certain that the basis sets used to represent the molecular orbitals are sufficiently large so that the states (especially the excited states) can be accurately modelled. Secondly, at room temperatures, the surface of the gold electrodes is not perfectly crystalline. We model this by repeating the calculations with randomly placed ad-atoms (see Fig. S16) that simulate deviations from the crystalline order. In Fig. S15, we can compare the results obtained for smaller basis set size and for the same basis set size but including add-atoms with the results obtained in the rest of the text. We can see that in both cases, the changes to both the transmission function and the local density of states are small, on the order of few percent of the magnitude of the respective observables.

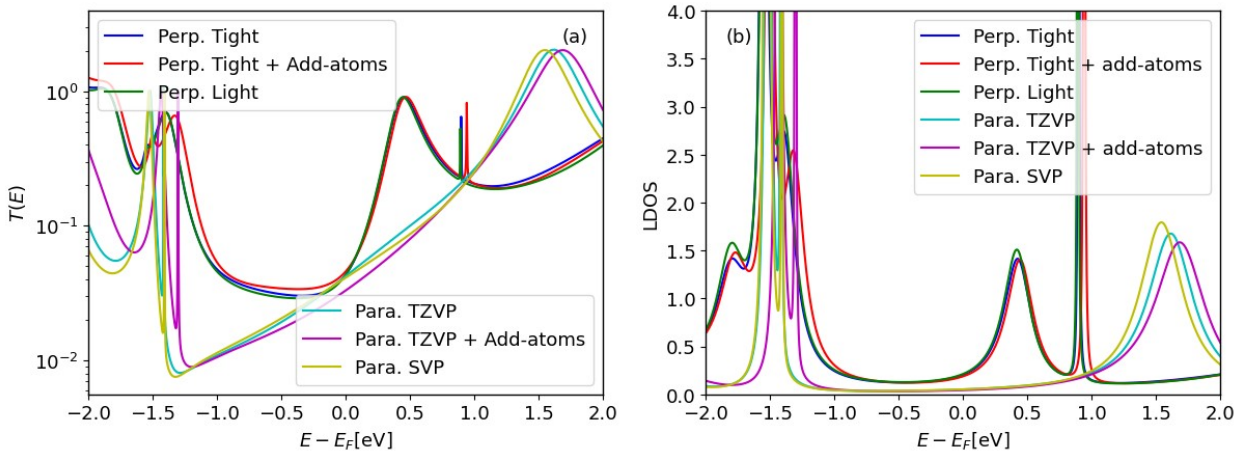

Figure S15: *The transmission function (a) and local density of states (b) on the iron ion at the centre of the ferrocene molecule for different basis sets and with the inclusion of add-atoms. Changes to both observables are small – on the order of few percent. The qualitative results of the ab-initio calculations are therefore numerically (basis) and configurationally (add-atoms) stable.*

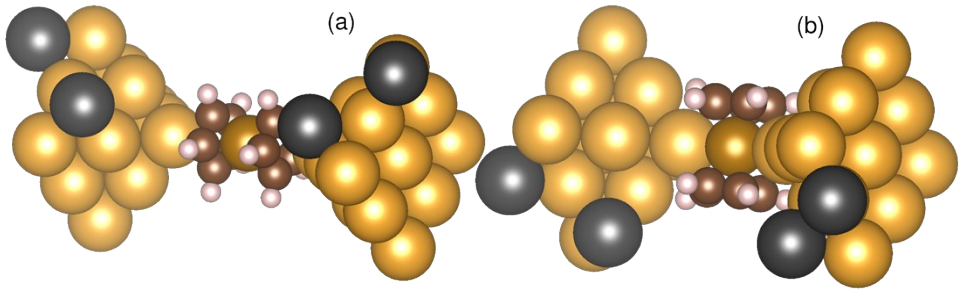

Figure S16: *The geometries of the parallel (a) and perpendicular (b) junctions with ad-atoms placed on the electrodes. Ad-atoms are gold atoms, here their color is changed to gray to explicitly differentiate them from the regular (crystalline) gold atoms.*

(i) Calculation of transmission function constrained to a single scattering state

The transmission function is calculated in the Landauer-Buttiker approach in the AITRANSS package, as described in the main text. This involves derivation of the transmission function as trace of the matrix product of matrices based on NEGFs of the extended molecule. Dropping the (orbital) indices for certain orbitals allows us to see the transmission function without the influence of the orbitals with given indices. Alternatively, all indices except one can be set to zero, leaving us with a single peak, corresponding to non-interfering transport through single orbital. Numerically, this is done by including a masking matrix M_{ij}, which has entries either 1 or 0, with 1 only at indices with orbitals to be considered for transmission, i.e.

$$T = \sum_{i,j} M_{ij} \Gamma_{L,ij} G_j \Gamma_{R,ji} G_i^c$$

where the symbols used have the same meaning as given in the AITRANSS package article[8] and the summation runs over indices of the non-equilibrium eigen states.

(j) Coordinates of Converged Junctions

We are including the xyz coordinate files of the junctions used for conductance and LDOS

```
49

AU 2.6 0.0 0.0
AU 4.635 2.035 0.0
AU 4.635 0.0 -2.035
AU 4.635 -2.035 0.0
AU 4.635 0.0 2.035
AU 6.67 4.07 0.0
AU 6.67 2.035 -2.035
AU 6.67 0.0 0.0
AU 6.67 2.035 2.035
AU 6.67 0.0 -4.07
AU 6.67 -2.035 -2.035
AU 6.67 -4.07 0.0
AU 6.67 -2.035 2.035
AU 6.67 0.0 4.07
C 0.97965951 0.72286369 -1.83333102
C 0.97965276 -0.72284304 -1.8333394
C -0.36393193 -1.16133116 -1.73942802
C -1.21474473 2.06e-05 -1.81068501
C -0.36392134 1.16136335 -1.73941294
H 1.83741061 1.36962039 -2.01043626
H 1.83739862 -1.36960559 -2.01044833
H -0.70582592 -2.19099436 -1.75493551
H -2.21956146 2.878e-05 -2.2709147
H -0.70580557 2.19102994 -1.75490815
FE 0.01542159 4.98e-06 3e-08
C -0.36392358 -1.1613507 1.73941577
C -1.21474471 -6.06e-06 1.81068505
C -0.36392968 1.16134382 1.73942527
C 0.97965417 0.72285316 1.83333784
C 0.97965812 -0.72285356 1.83333265
H -0.70580987 -2.19101658 1.75491323
H -2.21956146 -1.088e-05 2.2709147
H -0.7058216 2.19100772 1.75493052
H 1.83740143 1.36961424 2.01044514
H 1.83740782 -1.36961173 2.01043951
AU -2.6 0.0 0.0
AU -4.635 2.035 0.0
AU -4.635 0.0 2.035
AU -4.635 -2.035 0.0
AU -4.635 0.0 -2.035
AU -6.67 4.07 0.0
AU -6.67 2.035 2.035
AU -6.67 0.0 0.0
AU -6.67 2.035 -2.035
AU -6.67 0.0 4.07
AU -6.67 -2.035 2.035
AU -6.67 -4.07 0.0
AU -6.67 -2.035 -2.035
AU -6.67 0.0 -4.07
```

calculations in main text. For the perpendicular geometry of Ferrocene (FC) at distance 2.6 Å

For the parallel geometry of Ferrocene (FC) at distance 4.1 Å

AU 4.1000000000000005 0.0 0.0
AU 6.1349999999999945 2.034999999999999 0.0
AU 6.1349999999999945 0.0 -2.034999999999999
AU 6.1349999999999945 -2.034999999999999 0.0
AU 6.1349999999999945 0.0 2.034999999999999
AU 8.170000000000003 4.070000000000003 0.0
AU 8.170000000000003 2.034999999999999 -2.034999999999999
AU 8.170000000000003 0.0 0.0
AU 8.170000000000003 2.034999999999999 2.034999999999999
AU 8.170000000000003 0.0 -4.070000000000003
AU 8.170000000000003 -2.034999999999999 -2.034999999999999
AU 8.170000000000003 -4.070000000000003 0.0
AU 8.170000000000003 -2.034999999999999 2.034999999999999
AU 8.170000000000003 0.0 4.070000000000003
C -1.6275884823423405 1.1672011660639403 -0.3794940697340722
C -1.6280444640169234 1.9040681679270106e-06 -1.2275172039221152
C -1.6275938041695084 -1.1672002906265961 -0.37949638933260704
C -1.6272869449855327 -0.7214323180761611 0.992844894170462
C -1.6272841432496512 0.721430617767112 0.9928453696556596
H -1.6230710629197664 2.1995178676132316 -0.7146906088067383
H -1.6232334781413114 -9.218863237893784e-07 -2.312954673714635
H -1.6230798843302994 -2.1995158602355698 -0.7146947432813314
H -1.6234780155466357 -1.3589602783781292 1.8714272764475401
H -1.6234720284592095 1.358957808092817 1.8714292702044983
FE 6.0090768477092287e-05 -4.036063279545556e-06 -0.00023053059714474308
C 1.627267917833809 -0.7214326978809809 0.9928470583912591
C 1.6272658448969644 0.7214300848318275 0.992847393026095
C 1.6275718834970363 1.1672065716085678 -0.37949628146332515
C 1.6280369178532152 1.3411948043539458e-06 -1.2275256323366734
C 1.6275771453266477 -1.1672061010152217 -0.3794988757873471
H 1.6234914534695386 -1.3590035157746307 1.8714880936174583
H 1.6234862036312574 1.3590002848383538 1.8714900456060093
H 1.6230865555481842 2.1995915927532743 -0.7147139486369102
H 1.6232514060329768 -1.3748423732642777e-06 -2.3130380071454466
H 1.6230957422834067 -2.1995902276311665 -0.7147183111014612
AU -4.1000000000000005 0.0 0.0
AU -6.1349999999999945 2.034999999999999 0.0
AU -6.1349999999999945 0.0 2.034999999999999
AU -6.1349999999999945 -2.034999999999999 0.0
AU -6.1349999999999945 0.0 -2.034999999999999
AU -8.170000000000003 4.070000000000003 0.0
AU -8.170000000000003 2.034999999999999 2.034999999999999
AU -8.170000000000003 0.0 0.0
AU -8.170000000000003 2.034999999999999 -2.034999999999999
AU -8.170000000000003 0.0 4.070000000000003
AU -8.170000000000003 -2.034999999999999 2.034999999999999
AU -8.170000000000003 -4.070000000000003 0.0
AU -8.170000000000003 -2.034999999999999 -2.034999999999999
AU -8.170000000000003 0.0 -4.070000000000003

For anchoring group coupled 1,1′-bis(aminomethyl)ferrocene (FC-NH_2)

59

H	6.925502e+00	4.942298e+00	6.607842e+00
H	6.980205e+00	2.650830e+00	7.374509e+00
N	6.507916e+00	4.675867e+00	7.512306e+00
C	7.191464e+00	3.499583e+00	8.058416e+00
H	6.612877e+00	5.490762e+00	8.134631e+00
H	9.100405e+00	5.816601e+00	8.231419e+00
C	8.692103e+00	3.593483e+00	8.241950e+00
C	9.484256e+00	4.794415e+00	8.257599e+00
C	1.087128e+01	4.426156e+00	8.311816e+00
C	9.604039e+00	2.483432e+00	8.314512e+00
H	9.327490e+00	1.426561e+00	8.329731e+00
H	1.172283e+01	5.109442e+00	8.345576e+00
C	1.094514e+01	2.994194e+00	8.348136e+00
H	1.185701e+01	2.397103e+00	8.405771e+00
H	6.701868e+00	3.231766e+00	9.013912e+00
Fe	9.889768e+00	3.693187e+00	9.940453e+00
H	6.213784e+00	3.897110e+00	1.085850e+01
H	7.340496e+00	1.749985e+00	1.116580e+01
H	1.109847e+01	5.741479e+00	1.145433e+01
H	1.220093e+01	3.259619e+00	1.148205e+01
C	1.055004e+01	4.799452e+00	1.152599e+01
C	1.113528e+01	3.489383e+00	1.154051e+01
H	8.389237e+00	5.453417e+00	1.157986e+01
C	9.122281e+00	4.643879e+00	1.159113e+01
C	1.006820e+01	2.531723e+00	1.160680e+01
H	1.018658e+01	1.446202e+00	1.162325e+01
C	8.816670e+00	3.240499e+00	1.165267e+01
N	6.279121e+00	3.447924e+00	1.178355e+01
C	7.467251e+00	2.597673e+00	1.186954e+01
H	6.324841e+00	4.204410e+00	1.248176e+01
H	7.466900e+00	2.137877e+00	1.288214e+01
Au	6.377095e+00	3.697642e+00	5.526543e+00
Au	7.816057e+00	2.258680e+00	3.491543e+00
Au	7.816057e+00	5.136604e+00	3.491543e+00
Au	4.938133e+00	5.136604e+00	3.491543e+00
Au	4.938133e+00	2.258680e+00	3.491543e+00
Au	9.255020e+00	8.197173e-01	1.456543e+00
Au	9.255020e+00	3.697642e+00	1.456543e+00
Au	6.377095e+00	3.697642e+00	1.456543e+00
Au	6.377095e+00	8.197173e-01	1.456543e+00
Au	9.255020e+00	6.575566e+00	1.456543e+00
Au	6.377095e+00	6.575566e+00	1.456543e+00
Au	3.499171e+00	6.575566e+00	1.456543e+00
Au	3.499171e+00	3.697642e+00	1.456543e+00
Au	3.499171e+00	8.197173e-01	1.456543e+00
Au	6.377095e+00	3.697642e+00	1.376904e+01
Au	7.816057e+00	2.258680e+00	1.580404e+01
Au	7.816057e+00	5.136604e+00	1.580404e+01
Au	4.938133e+00	5.136604e+00	1.580404e+01
Au	4.938133e+00	2.258680e+00	1.580404e+01
Au	9.255020e+00	8.197173e-01	1.783904e+01
Au	9.255020e+00	3.697642e+00	1.783904e+01
Au	6.377095e+00	3.697642e+00	1.783904e+01
Au	6.377095e+00	8.197173e-01	1.783904e+01
Au	9.255020e+00	6.575566e+00	1.783904e+01
Au	6.377095e+00	6.575566e+00	1.783904e+01
Au	3.499171e+00	6.575566e+00	1.783904e+01
Au	3.499171e+00	3.697642e+00	1.783904e+01
Au	3.499171e+00	8.197173e-01	1.783904e+01

For anchoring group coupled 1,1′-dicyanoferrocene (FC-CN)

51

N	5.404041e+00	2.996933e+00	1.142563e+01
C	6.558563e+00	3.204079e+00	1.148250e+01
C	7.953150e+00	3.472143e+00	1.151889e+01
H	8.002465e+00	5.730986e+00	1.152239e+01
C	8.550918e+00	4.788277e+00	1.153238e+01
C	9.970659e+00	4.614990e+00	1.153808e+01
C	9.017297e+00	2.492573e+00	1.154076e+01
H	8.883532e+00	1.409709e+00	1.154121e+01
C	1.025784e+01	3.208797e+00	1.154291e+01
H	1.070626e+01	5.419941e+00	1.156112e+01
H	1.125240e+01	2.761924e+00	1.157012e+01
Fe	9.119944e+00	3.715408e+00	1.317074e+01
H	7.944199e+00	5.714581e+00	1.479115e+01
C	8.507333e+00	4.781622e+00	1.479786e+01
C	9.000109e+00	2.493293e+00	1.480037e+01
H	8.866322e+00	1.410988e+00	1.480060e+01
C	7.925030e+00	3.458802e+00	1.480322e+01
H	1.065847e+01	5.437564e+00	1.480905e+01
H	1.123077e+01	2.778390e+00	1.481242e+01
C	9.931441e+00	4.624671e+00	1.481414e+01
C	1.023332e+01	3.220722e+00	1.481572e+01
C	6.537727e+00	3.151517e+00	1.482012e+01
N	5.394238e+00	2.887504e+00	1.486477e+01
Au	5.083522e+00	3.184248e+00	9.412057e+00
Au	3.644559e+00	1.745285e+00	7.377057e+00
Au	6.522484e+00	1.745285e+00	7.377057e+00
Au	6.522484e+00	4.623210e+00	7.377057e+00
Au	3.644559e+00	4.623210e+00	7.377057e+00
Au	2.205597e+00	3.063232e-01	5.342057e+00
Au	5.083522e+00	3.063232e-01	5.342057e+00
Au	5.083522e+00	3.184248e+00	5.342057e+00
Au	2.205597e+00	3.184248e+00	5.342057e+00
Au	7.961446e+00	3.063232e-01	5.342057e+00
Au	7.961446e+00	3.184248e+00	5.342057e+00
Au	7.961446e+00	6.062172e+00	5.342057e+00
Au	5.083522e+00	6.062172e+00	5.342057e+00
Au	2.205597e+00	6.062172e+00	5.342057e+00
Au	5.083522e+00	3.184248e+00	1.687838e+01
Au	3.644559e+00	1.745285e+00	1.891338e+01
Au	6.522484e+00	1.745285e+00	1.891338e+01
Au	6.522484e+00	4.623210e+00	1.891338e+01
Au	3.644559e+00	4.623210e+00	1.891338e+01
Au	2.205597e+00	3.063232e-01	2.094838e+01
Au	5.083522e+00	3.063232e-01	2.094838e+01
Au	5.083522e+00	3.184248e+00	2.094838e+01
Au	2.205597e+00	3.184248e+00	2.094838e+01
Au	7.961446e+00	3.063232e-01	2.094838e+01
Au	7.961446e+00	3.184248e+00	2.094838e+01
Au	7.961446e+00	6.062172e+00	2.094838e+01
Au	5.083522e+00	6.062172e+00	2.094838e+01
Au	2.205597e+00	6.062172e+00	2.094838e+01

(k) Binding energy of anchoring group coupled FC-NH_2 and FC-CN

Table S2: *Binding energy of FC-NH_2 and FC-CN*

Molecular system	Binding energy of Anchoring geometry
1,1′-bis(aminomethyl)ferrocene (FC-NH_2)	-1.20 eV
1,1′-dicyanoferrocene (FC-CN)	-1.13 eV

References:

(1) Teresa González, M.; Wu, S.; Huber, R.; Van Der Molen, S. J.; Schönenberger, C.; Calame, M. Electrical Conductance of Molecular Junctions by a Robust Statistical Analysis. *Nano Lett* **2006**, *6* (10), 2238–2242. https://doi.org/10.1021/nl061581e.

(2) Martin, C. A.; Ding, D.; Sørensen, J. K.; Bjørnholm, T.; Van Ruitenbeek, J. M.; Van Der Zant, H. S. J. Fullerene-Based Anchoring Groups for Molecular Electronics. *J Am Chem Soc* **2008**, *130* (40), 13198–13199. https://doi.org/10.1021/ja804699a.

(3) Quek, S. Y.; Kamenetska, M.; Steigerwald, M. L.; Choi, H. J.; Louie, S. G.; Hybertsen, M. S.; Neaton, J. B.; Venkataraman, L. Mechanically Controlled Binary Conductance Switching of a Single-Molecule Junction. *Nat Nanotechnol* **2009**, *4* (4), 230–234. https://doi.org/10.1038/nnano.2009.10.

(4) Chen, F.; Li, X.; Hihath, J.; Huang, Z.; Tao, N. Effect of Anchoring Groups on Single-Molecule Conductance: Comparative Study of Thiol-, Amine-, and Carboxylic-Acid-Terminated Molecules. *J Am Chem Soc* **2006**, *128* (49), 15874–15881. https://doi.org/10.1021/ja065864k.

(5) Hong, W.; Manrique, D. Z.; Moreno-García, P.; Gulcur, M.; Mishchenko, A.; Lambert, C. J.; Bryce, M. R.; Wandlowski, T. Single Molecular Conductance of Tolanes: Experimental and Theoretical Study on the Junction Evolution Dependent on the Anchoring Group. *J Am Chem Soc* **2012**, *134* (4), 2292–2304. https://doi.org/10.1021/ja209844r.

(6) Makk, P.; Tomaszewski, D.; Martinek, J.; Balogh, Z.; Csonka, S.; Wawrzyniak, M.; Frei, M.; Venkataraman, L.; Halbritter, A. Correlation Analysis of Atomic and Single-Molecule Junction Conductance. *ACS Nano* **2012**, *6* (4), 3411–3423. https://doi.org/10.1021/nn300440f.

(7) Perrin, M. L.; Martin, C. A.; Prins, F.; Shaikh, A. J.; Eelkema, R.; van Esch, J. H.; van Ruitenbeek, J. M.; van der Zant, H. S. J.; Dulić, D. Charge Transport in a Zinc-Porphyrin Single-Molecule Junction. *Beilstein J Nanotechnol* **2011**, *2* (1), 714–719. https://doi.org/10.3762/bjnano.2.77.

(8) Arnold, A.; Weigend, F.; Evers, F. Quantum Chemistry Calculations for Molecules Coupled to Reservoirs: Formalism, Implementation, and Application to Benzenedithiol. *J Chem Phys* **2007**, *126* (17). https://doi.org/10.1063/1.2716664.

(9) Bagrets, A. Spin-polarized electron transport across metal–organic molecules: a density functional theory approach. *J. Chem. Theory Comput.* **2013**, *9*, 2801–2815.